A CMOS-Compatible Hybrid Plasmonic Slot Waveguide With Enhanced Field Confinement

Xiao, Jing; Wei, Qi-Qin; Yang, Daoguo; Zhang, Ping; He, Ning; Zhang, Guo Qi; Ren, Tian-Ling; Chen, Xian-Ping

DOI
10.1109/LED.2016.2531990

Publication date
2016

Document Version
Final published version

Published in
IEEE Electron Device Letters

A CMOS-Compatible Hybrid Plasmonic Slot Waveguide With Enhanced Field Confinement

Jing Xiao, Qi-Qin Wei, Dao-Guo Yang, Ping Zhang, Ning He, Guo-Qi Zhang, *Fellow, IEEE*, Tian-Ling Ren, *Senior Member, IEEE*, and Xian-Ping Chen

***Abstract*— The emerging field of nanophotonics requires plasmonic devices to be fully compatible with semiconductor fabrication techniques. However, very few feasible practical structures exist at present. Here, we propose a CMOS-compatible hybrid plasmonic slot waveguide (HPSW) with enhanced field confinement. Our simulation results show that the HPSW exhibits significantly enhanced field confinement as compared with the traditional low-index slot waveguides and the hybrid metal dielectric slot waveguides. By controlling the thicknesses of different layers, an optimized HPSW structure with a better tradeoff between field confinement and propagation length has been simultaneously achieved.**

***Index Terms*— Hybrid plasmonic slot waveguide, field confinement, multi-layer structure.**

I. Introduction

SURFACE plasmon polaritons (SPPs) have attracted significant research interest in the past three decades because of their remarkable properties, such as energy asymptote in dispersion curve, resonance, field enhancement, large surface area, bulk sensitivity, and subwavelength confinement [1]–[4]. However, semiconductor based plasmonics have to face a fundamental challenge-high optical loss, especially when high-permittivity dielectric materials such as semiconductors are involved [2], [4]. To overcome this drawback, hybrid plasmonic waveguides (HPWs) have been proposed, which are capable of providing a better tradeoff between field confinement and propagation loss, as compared with their conventional plasmon waveguiding counterparts [3], [5]–[8]. The coupling between the dielectric and the plasmonic modes enables HPWs to confine light at the nanoscale domain and allow effective subwavelength transmission in non-metallic regions [4], [9], [10]. The rapidly growing family of HPWs can be divided into two main categories: (i) conventional configurations that comprise a high-index dielectric nanowire separated from a metal surface by a nanoscale dielectric gap and (ii) silicon-based waveguides composed of truncated metallic strips deposited over silicon-on-insulator (SOI) substrates [4]. In order to further improve their guiding performance, a number of modified HPWs structures have been proposed [11]–[14]. Nevertheless, the tradeoff between modal attenuation and propagation distance still exists in most of these modified structures.

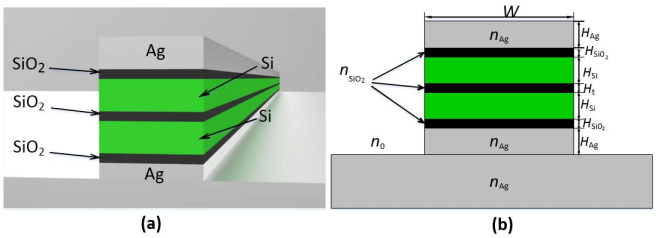

Fig. 1. (a) 3D and (b) 2D cross-section geometries of the HPSW.

By using a finite element method (FEM), we introduce simulation results of a CMOS-compatible HPSW, which is capable of not only providing enhanced field confinement but also balancing the propagation distance and modal size. This HPSW consists of a low-refractive-index slot embedded between two symmetrical hybrid plasmonic strips with a metal-insulator-semiconductor-slot-semiconductor-insulator-metal multi-layer configuration. Our results show that the HPSW can provide strong field enhancement and ultra-high-mode confinement in one dimension while reducing propagation loss. In addition, the multi-layer structure is fully compatible with semiconductor process and could lead to real plasmonics and photonics on a nanoscale.

II. Proposed Waveguide Structure and Simulations

The three-dimensional (3D) and two-dimensional (2D) cross-section geometries for HPSW are shown in Figs. 1(a) and 1(b), respectively. The metal layers on the top and the bottom are Ag, and the semiconductor and low-index insulator layers are Si and SiO_2, respectively. To facilitate the description, we denote the width of the hybrid strip as W, the thicknesses of Ag layers, Si layers, SiO_2 layers between Ag and Si layers, and SiO_2 layer in the center as H_{Ag}, H_{Si}, H_{SiO_2}, and H_t, respectively. The modal properties of this new configuration were investigated and analysed by employing the commercial software COMSOL. In all simulations,

Manuscript received January 7, 2016; revised January 14, 2016, January 25, 2016, February 1, 2016, and February 2, 2016; accepted February 3, 2016. Date of publication February 24, 2016; date of current version March 22, 2016. This work was supported in part by the National Natural Science Foundation of China under Grant 51303033, Grant 61434001, and Grant 61434004 and in part by the Guangxi Natural Science Foundation under Grant 2014GXNSFCB118004. The review of this letter was arranged by Editor E. A. Gutiérrez-D.

J. Xiao, Q.-Q Wei, D.-G. Yang, P. Zhang, and N. He are with the School of Mechanical and Electrical Engineering, Guilin University of Electronic Technology, Guilin 541004, China.

G.-Q. Zhang is with the Delft Institute of Microsystems and Nanoelectronics, Delft University of Technology, Delft 2628 CD, The Netherlands.

T.-L. Ren is with the Institute of Microelectronics, Tsinghua University, Beijing 100084, China.

X.-P. Chen is with the School of Mechanical and Electrical Engineering, Guilin University of Electronic Technology, Guilin 541004, China, also with the College of Opto-Electronic Engineering, Chongqing University, Chongqing 400044, China, and also with the Institute of Microelectronics, Tsinghua University, Beijing 100084, China (e-mail: xianpingchen@tsinghua.edu.cn).

Color versions of one or more of the figures in this letter are available online at http://ieeexplore.ieee.org.

Digital Object Identifier 10.1109/LED.2016.2531990

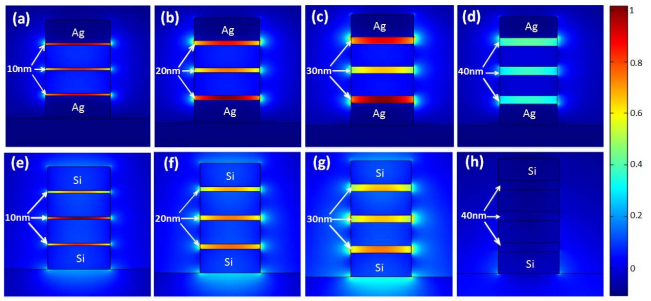

Fig. 2. The cross-section of the electrical field distributions for both HPSWs [(a)-(d)] and LISWs [(e)-(h)] with different thickness of SiO_2 layers at 10 nm, 20 nm, 30 nm, and 40 nm, respectively.

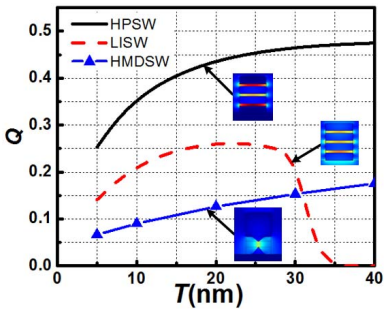

Fig. 3. Dependence of the confinement factor (Q) for HPSWs, LISWs and HMDSWs with the thickness of SiO_2 layer ranging from 5 to 40 nm.

a wavelength λ of 1550 nm was used. The refractive indices of Si, SiO_2, air, and Ag were taken as $n_{Si} = 3.45$, $n_{SiO_2} = 1.45$, $n_o = 1$, and $n_{Ag} = 0.1453 + 11.3587i$ [15], respectively. The H_{Ag} and W were chosen respectively as 50 nm and 200 nm to ensure a single transverse magnetic SPP mode propagation [5]. The calculation region was given with scattering boundary conditions. A convergence analysis was conducted to ensure that the meshing, boundary conditions and associated calculation parameters were sound [2].

III. Results and Discussion

This investigation is started by comparing the field confinement capability of HPSW structure with the traditional low-index slot waveguides (LISWs) [16], [17]. The thicknesses of SiO_2 layers H_{SiO_2} and H_t are assumed to be the same (i.e., $H_{SiO_2} = H_t = T$). Fig. 2 shows the corresponding electrical field distribution of HPSWs and LISWs proposed by Li *et al.* [14] with the thicknesses of SiO_2 layer at 10 nm, 20 nm, 30 nm, and 40 nm, respectively. It is remarkable to find that the field confinement capability of both HPSWs and LISWs shows a decline with the increase of the thickness of SiO_2 layer. We also observe that the HPSWs have much better field confinement capability than that of LISWs [14], [15]. For LISWs, the optical field cannot be trapped in the low-index layers when the thickness of SiO_2 layer exceeds 35 nm.

Towards a better understanding of the model characteristic, we analyze the dependence of the optical confinement of HPSWs, hybrid metal dielectric slot waveguides (HMDSWs) [16] and LISWs [14], [15]. For this purpose, a parameter called confinement factor is introduced and defined as: $Q = P_1/P_2$, where P_1 is the power density of the low-index layer and P_2 is the power density of all the layers. The confinement factor Q versus the thickness of the SiO_2 layer T is plotted in Fig. 3. The label T for HMDSWs refers to the thickness of SiO_2 between two bow-tie structures [18]. It is important to note that the value of Q for HPSWs is much higher than that of both HMDSWs and LISW at the range of T from 5 to 40 nm. For example, at $T = 5$ nm the value of Q for HPSWs is about 0.25, but for LISWs and HMDSWs, the Q values are only about 0.14 and 0.05, respectively. Along with the increase of T from 5 to 40 nm, the values of Q for both HPSWs and HMDSWs are increased. For LISWs, the value of Q has a similar trend at the range of T from 5 to 20 nm. At $T = 20$ nm, the values of Q for LISWs and HMDSWs are 0.253 and 0.13, respectively; but for HPSWs, it is higher than 0.44. When T increases from 27 to 35 nm, the value of Q for LISWs drops sharply from 0.25 to 0. The HPSWs can provide better Q because of their enhanced optical confinement ability which can be attributed to the combination of the two symmetrical hybrid plasmonic strips. The substantial amount of power confined in such nanoscale regions extends the capability of the HPSW structures for various applications such as nonlinear interactions, sensing, and optical force [19].

For practical realizations of the HPSW model, optimization design is performed to find out a better tradeoff between the field confinement and propagation length: $L = \lambda/[4\pi\ Im(n_{eff})]$, where n_{eff} is the complex modal effective index, and $Im(n_{eff})$ is the imaginary part of n_{eff}. To compare the performances of different HPSW configurations, the parameters-figure of merit (FOM) and the normalized effective mode area (A_{eff}/A_0) [2], are introduced. FOM $= L/[2(A_{eff}/\pi)^{1/2}]$, A_0 is the diffraction-limited mode area in free space and can be defined as $\lambda^2/4$, and A_{eff} is the effective mode area [2], which can be calculated by:

$$A_{eff} = \left[\iint W(\mathbf{r})dA\right]/\{\max(W(\mathbf{r})\} \tag{1}$$

in which the electromagnetic energy density $W(r)$ is defined as

$$W(\mathbf{r}) = \frac{1}{2}Re\left\{\frac{d[\omega\varepsilon(\mathbf{r})]}{d\omega}\right\}|E(\mathbf{r})|^2 + \frac{1}{2}\mu_0|H(\mathbf{r})|^2 \tag{2}$$

where $E(r)$ and $H(r)$ are the electric and magnetic fields, $\varepsilon(r)$ is the electric permittivity, and μ_0 is the vacuum permeability. In the following study, we vary the thickness of the center low-index layer H_t from 5 to 60 nm, and the thickness of SiO_2 between Ag and Si layers is fixed at 20 nm. To control the optical confinement properties of HPSWs, the thicknesses of high-index layers (H_{Si}) are set at 50, 75, 100, and 125 nm, respectively. Figs. 4(a)-(d) schematically show the electric field distributions of HPSWs with different H_t at 10, 30, 50, and 80 nm, respectively. The intensity of the corresponding electric field profiles in the y-axis direction (E_y) with different H_t are plotted in Figs. 4(e)-(h), respectively. They clearly show that E_y is decreased with the increase of H_t. Therefore, we further analyze the effect of H_t and H_{Si} on Im(n_{eff}), L, A_{eff}/A_0, and FOM as shown in Figs. 5(a)-(d), respectively. It can be easily seen that when $H_t < 80$ nm, $Im(n_{eff})$ is increased as

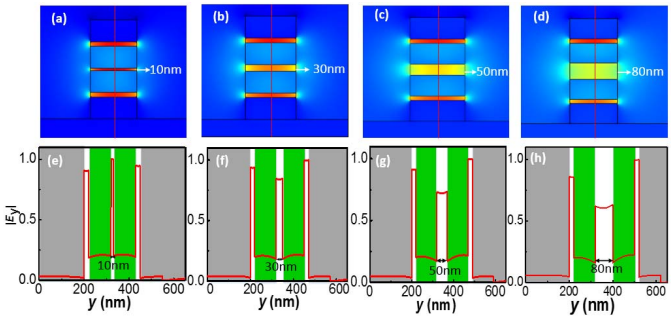

Fig. 4. (a)-(d) The cross section of electric field distributions and (e)-(h) The corresponding field profiles in y-axis direction (Ey) for HPSWs with different H_t at 10 nm, 30 nm, 50 nm, and 80 nm, respectively, when $H_{SiO_2} = 20$ nm.

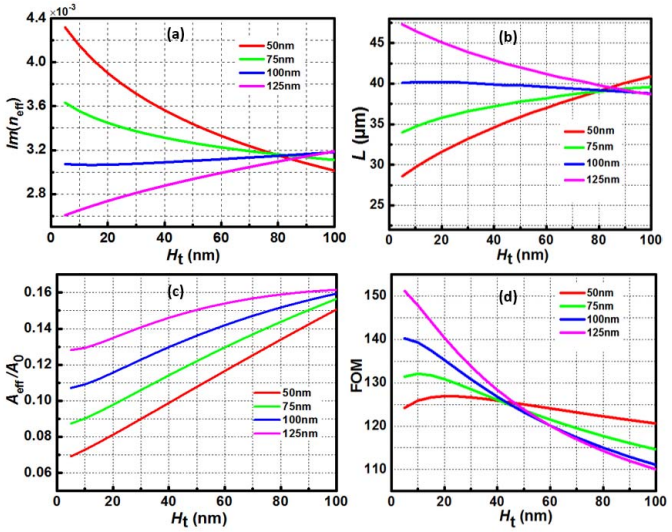

Fig. 5. Dependence of (a) *Im* (n_{eff}), (b) L, (c) A_{eff}/A_0, and (d) FOM on the thickness of the center SiO_2 layer (H_t) of the proposed HPSW model with different H_{si} at 50, 75, 100, and 125 nm, respectively.

H_{Si} decreases, implying that the increase of H_{Si} will help to reduce the transmission loss [see Fig. 5(a)]. By contrast, when $H_t < 80$ nm, the increase of H_{Si} will improve the propagation length as indicated in Fig. 5(b). We also observe that A_{eff}/A_0 can be enlarged by increasing H_{Si} or H_t or both of them as shown in Fig. 5(c), which means the field confinement capability has a negative dependence of H_{Si} or H_t or both of them. Using the L/H_t data in Fig. 5(b) together with the $(A_{\text{eff}}/A_0)/H_t$ data in Fig. 5(c), it is possible to derive the relationship between FOM and H_t for each H_{Si} [see Fig. 5(d)]. Based on the data of Fig. 5(d), the optimized HPSW configuration with a better tradeoff between field confinement ($A_{\text{eff}} = 0.127\ \mu m^2$) and propagation length ($L = 46.7\ \mu$m) can be achieved when $W = 200$ nm, $H_{Si} = 125$ nm, $H_t = 10$ nm, $H_{SiO_2} = 10$ nm. In this case, n_{eff} is 2.273.

IV. Conclusion

In conclusion, we have proposed a new CMOS-compatible HPSW structure which combines two symmetrical hybrid plasmonic strips through FEM analysis. Simulation data of electrical field distribution and confinement factor demonstrate that the HPSW can provide much better field confinement capability as compared with the traditional LISWs and HMDSWs. The optimized HPSW configuration with a better tradeoff between field confinement and propagation length has been achieved through adjusting the thicknesses of the different layers. The proposed HPSW structure is fully compatible with semiconductor fabrication techniques and could lead to truly nanoscale semiconductor-based plasmonics, photonics and components with high-performance.

References

[1] R. Kirchain and L. Kimerling, "A roadmap for nanophotonics," *Nature Photon.*, vol. 1, pp. 303–305, Jun. 2007, doi: 10.1038/nphoton.2007.84.
[2] R. F. Oulton, V. J. Sorger, D. A. Genov, D. F. P. Pile, and X. Zhang, "A hybrid plasmonic waveguide for subwavelength confinement and long-range propagation," *Nature Photon.*, vol. 2, no. 8, pp. 496–500, Aug. 2008, doi: 10.1038/nphoton.2008.131.
[3] V. J. Sorger, Z. Ye, R. F. Oulton, Y. Wang, G. Bartal, X. Yin, and X. Zhang, "Experimental demonstration of low-loss optical waveguiding at deep sub-wavelength scales," *Nature Commun.*, vol. 2, p. 331, May 2011, doi: 10.1038/ncomms1315.
[4] Y. Bian and Q. Gong, "Bow-tie hybrid plasmonic waveguides," *J. Lightw. Technol.*, vol. 32, no. 23, pp. 4504–4509, Dec. 1, 2014, doi: 10.1109/JLT.2014.2359916.
[5] H.-S. Chu, E.-P. Li, P. Bai, and R. Hegde, "Optical performance of single-mode hybrid dielectric-loaded plasmonic waveguide-based components," *Appl. Phys. Lett.*, vol. 96, p. 221103, May 2010, doi: 10.1063/1.3437088.
[6] Y. Zhao and L. Zhu, "Coaxial hybrid plasmonic nanowire waveguides," *J. Opt. Soc. Amer. B*, vol. 27, pp. 1260–1265, Jun. 2010, doi: 10.1364/JOSAB.27.001260.
[7] H. Benisty and M. Besbes, "Plasmonic inverse rib waveguiding for tight confinement and smooth interface definition," *J. Appl. Phys.*, vol. 108, p. 063108, Sep. 2010, doi: 10.1063/1.3478746.
[8] Y. Bian and Q. Gong, "Long-range hybrid ridge and trench plasmonic waveguides," *Appl. Phys. Lett.*, vol. 104, p. 251115, Jun. 2014, doi: 10.1063/1.4885834.
[9] L. Chen, X. Li, G. Wang, W. Li, S. Chen, L. Xiao, and D. Gao, "A silicon-based 3-D hybrid long-range plasmonic waveguide for nanophotonic integration," *J. Lightw. Technol.*, vol. 30, no. 1, pp. 163–168, Jan. 1, 2012. doi: 10.1109/JLT.2011.2179008.
[10] Y. Bian and Q. Gong, "Metallic-nanowire-loaded silicon-on-insulator structures: A route to low-loss plasmon waveguiding on the nanoscale," *Nanoscale*, vol. 7, pp. 4415–4422, Mar. 2015, doi: 10.1039/c4nr06890d.
[11] L. Gao, L. Tang, F. Hu, R. Guo, X. Wang, and Z. Zhou, "Active metal strip hybrid plasmonic waveguide with low critical material gain," *Opt. Exp.*, vol. 20, pp. 11487–11495, May 2012, doi: 10.1364/OE.20.011487.
[12] L. Gao, Y. Huo, J. S. Harris, and Z. Zhou, "Ultra-compact and low-loss polarization rotator based on asymmetric hybrid plasmonic waveguide," *IEEE Photon. Technol. Lett.*, vol. 25, no. 21, pp. 2081–2084, Nov. 1, 2013, doi: 10.1109/LPT.2013.2281425.
[13] S. Zhu, G.-Q. Lo, J. Xie, and D.-L. Kwong, "Toward athermal plasmonic ring resonators based on Cu-TiO_2-Si hybrid plasmonic waveguide," *IEEE Photon. Technol. Lett.*, vol. 25, no. 12, pp. 1161–1164, Jun. 15, 2013, doi: 10.1109/LPT.2013.2261804.
[14] M. Li, C. L. Zou, X.-F. Ren, X. Xiong, Y.-J. Cai, G.-P. Guo, L.-M. Tong, and G.-C. Guo, "Transmission of photonic quantum polarization entanglement in a nanoscale hybrid plasmonic waveguide," *Nano Lett.*, vol. 15, pp. 2380–2384, Apr. 2015, doi: 10.1021/nl504636x.
[15] P. B. Johnson and R. W. Christy, "Optical constants of the noble metals," *Phys. Rev. B*, vol. 6, no. 12, pp. 4370–4379, Dec. 1972, doi: 10.1103/PhysRevB.6.4370.
[16] N.-N. Feng, J. Michel, and L. C. Kimerling, "Optical field concentration in low-index waveguides," *IEEE J. Quantum Electron.*, vol. 42, no. 9, pp. 885–890, Sep. 2006, doi: 10.1109/JQE.2006.880061.
[17] D. Dai and S. He, "Low-loss hybrid plasmonic waveguide with double low-index nano-slots," *Opt. Exp.*, vol. 18, pp. 17958–17966, Aug. 2010. doi: 10.1364/OE.18.017958.
[18] Y. Bian and Q. Gong, "Highly confined guiding of low-loss plasmon waves in hybrid metal-dielectric slot waveguides," *Nanotechnology*, vol. 25, pp. 345201-1–345201-11, Aug. 2014, doi: 10.1088/0957-4484/25/34/345201.
[19] K. J. Savage, M. M. Hawkeye, R. Esteban, A. G. Borisov, J. Aizpurua, and J. J. Baumberg, "Revealing the quantum regime in tunnelling plasmonics," *Nature*, vol. 491, pp. 574–577, Nov. 2012, doi: 10.1038/nature11653.